

Contents lists available at ScienceDirect

Nano Today

journal homepage: www.elsevier.com/locate/nanotoday





Cucurbituril regulated nano-supramolecular topological transform and reversible multicolor luminescent hydrogel for information encryption

Jing Kong ^{a,b,1}, Shuang-Qi Song ^{a,b,1}, Man Huo ^{a,b}, Chen Zhang ^{a,b}, Chu-Han Liu ^{a,b}, Yu Liu ^{a,b,*}

- ^a College of Chemistry, State Key Laboratory of Elemento Organic Chemistry, Nankai University, Tianjin 300071, PR China
- ^b Collaborative Innovation Center of Chemical Science and Engineering (Tianjin), Nankai University, Tianjin 300071, PR China

ARTICLE INFO

Keywords:
Supramolecular cascade assembly
Multicolor luminescence
Cucurbituril
Energy transfer
Information encryption

ABSTRACT

Herein, we report a multicolor supramolecular polyrotaxane hydrogel constructed by in situ polymerization of alkenyl-alkyl-modified pyrene pyridinium salt (PPD), cucurbit[n]urils (CB[n]s, n=7, 8), acrylamide (AM), and double bond-modified spiropyran (SP), which can achieve reversible multicolor luminescence from blue to red by light control. Benefiting from the spatial confinement of CB[n]s, PPD is encapsulated by the cavity of CB[7]/ CB[8] in a stoichiometric 1:2 or n:n to form the nanoparticles and nanofibers, and cascade assembly with the sulfobutylether- β -cyclodextrin (SBE- β CD) to form nanosheets and nanorods respectively, achieving the CB[n]-regulated supramolecular topological transform. Especially, in situ multi-component polymerization of CB[n]/ PPD/SP/AM achieves reversible multicolor supramolecular polyrotaxane luminescent hydrogel driven by light fuel, which can be effectively applied to information encryption as well as erasable ink through fluorescence resonance energy transfer (FRET) from PPDCCB[n] to SP. Therefore, the present research provides an effective approach for in situ polymerization to construct supramolecular soft materials for photo-controlled reversible multicolor luminescence.

Introduction

Taking advantage of spatial confinement of macrocyclic compounds, supramolecular cascade assembly to induce or enhance the luminescence of organic chromophore through noncovalent interactions such as hydrogen bonding[1-4], host-guest inclusion[5-8], metal-ligand coordination[9–12], and in situ polymerization [13] has become one of the research hotspots and a variety of stimulus-response systems have been successfully developed for application in information encryption [14-17], biosensing[18-22], energy transfer[23-26], molecular recognition[27,28], and hydrogels[29-31]. Typically, cascade supramolecular systems consist of two or more supramolecular macrocycles assembled with luminescent guest molecules to achieve stimulus response through luminescence driven by light fuel, temperature, pH, and mechanical force [32–38]. Among the various macrocycles, cucurbit [n]urils (CB[n]s, n = 7, 8) with rigid cavities can induce molecular folding[39,40] and molecular dimerization[41,42] through host-guest interaction, which can effectively and significantly improve the

luminescent behavior of guest molecules. For example, Ni and co-workers achieved multicolor luminescence, especially white light emission, in a single solution by simply adjusting the amount of CB[8] added, achieving the white light emission by a balanced mixture of the guest's intrinsic blue luminescence and the assembly's yellow luminescence. Moreover, the system exhibited a prolonged fluorescence lifetime and high quantum yield, maintaining efficient luminescent performance across various concentrations, which provided novel insights for the development of intelligent and tunable luminescent materials, particularly in the fields of optoelectronic devices and fluorescence sensors [43]. Multiply charged macrocycles, such as sulfobutylether-β-cyclodextrin (SBE-βCD)[44] or sulfonatocalix[4]arene[45] were used as secondary building blocks due to their ability to further assemble with the host-guest complex by hydrophobic cavities and electrostatic interaction, which can not only avoid the quenching of the fluorophores but also change the luminescence behavior of the fluorophores. Our group reported the SBE-βCD induced directional aggregation of cyanovinylene derivatives into nanorods, achieving UV-vis absorption and

^{*} Corresponding author at: College of Chemistry, State Key Laboratory of Elemento Organic Chemistry, Nankai University, Tianjin 300071, PR China. *E-mail address:* yuliu@nankai.edu.cn (Y. Liu).

 $^{^{\}rm 1}\,$ J. Kong and S. Q. Song contributed equally to this work

near-infrared fluorescence red-shift. Under alkaline conditions, the system showed reversible fluorescence blue-shift and 90-fold intensity enhancement, demonstrating reversible acid-base responsibility, which provided a new strategy for constructing intelligent fluorescent sensor devices[46]. Beyond pH-responsive systems, light-responsive supramolecular assemblies have also advanced rapidly in recent years[47-49]. Our group developed a light-responsive supramolecular hydrogel via cascade assembly of Laponite (LP) with CB[7]-encapsulated dicyanostilbene derivatives, which exhibited fluorescence enhancement and a 3D gel network at high LP concentrations. Further integration of fluorophores enabled reversible red/green chromatic switching, allowing self-erasing information encryption and anti-counterfeiting[50]. However, macrocyclic hosts regulated supramolecular topological morphology transform, especially pseudorotaxane in situ polymerization to construct supramolecular reversible multicolor luminescent hydrogel using cascade assembly strategies are rare reports to the best of our knowledge.

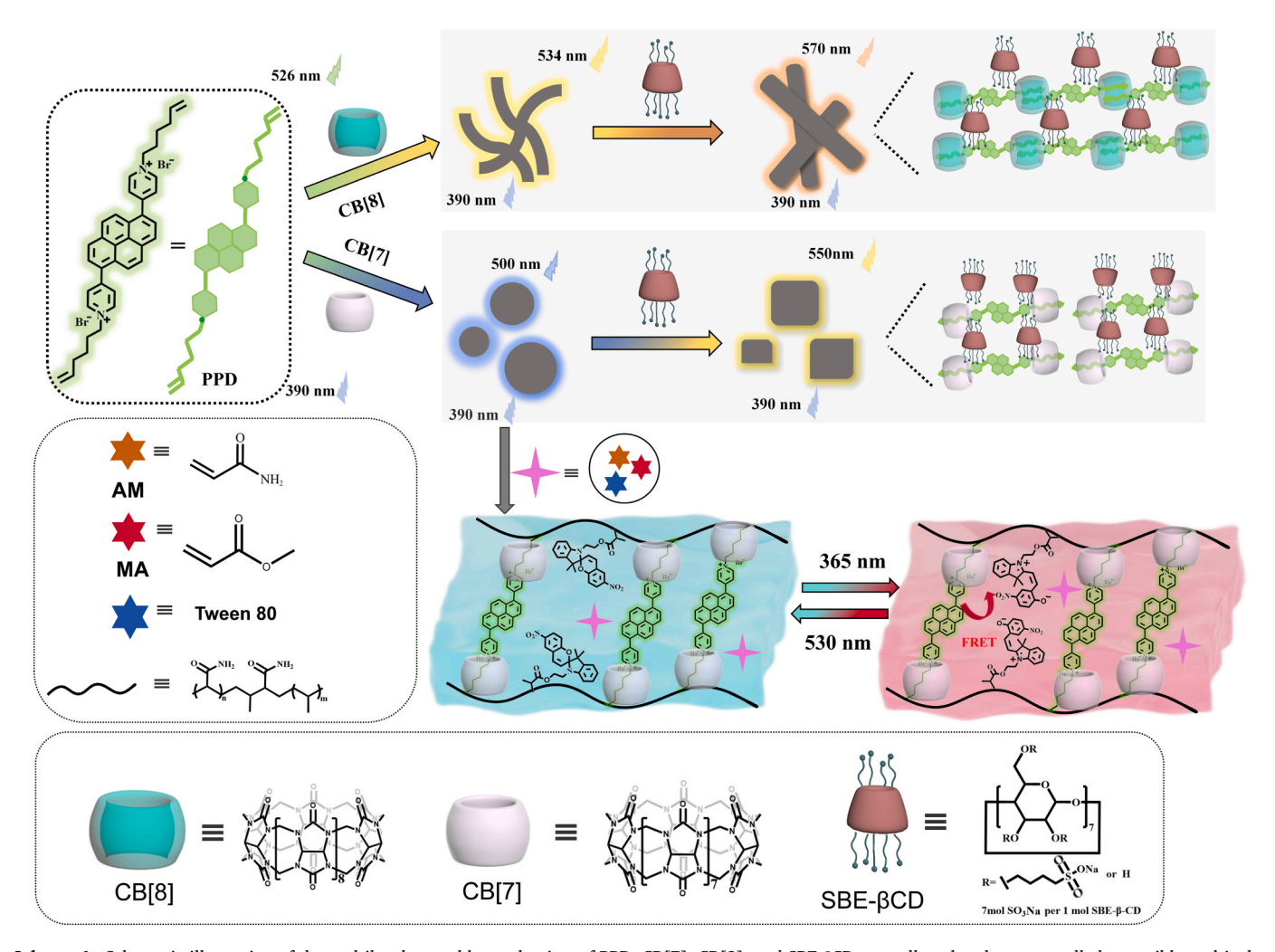
Herein, we reported the construction of multicolored fluorescence emission supramolecular polyrotaxane hydrogel based on alkenyl-alkyl modified pyrenyl pyridine salts (PPD), CB[n]s, acrylamide (AM), and double bond-modified spiropyran (SP) (Scheme 1). CB[7] confined PPD enhanced the fluorescence, and emission was blue-shifted from 526 nm to 500 nm, which the quantum yield increased from 54.65 % to 74.86 %. However, the fluorescence emission was red-shifted from 526 nm to 534 nm while encapsulated by CB[8], and the quantum yield was up to 64.43 %, and nanoparticles and nanofibers were formed, respectively.

Subsequently, when the cascade assembled with SBE-βCD, not only was the emission of PPD⊂CB[7]/CB[8] assembly further red-shifted, but also topological architectures underwent secondary variation to form nanosheets and nanorods, respectively. Furthermore, by copolymerizing CB [7]/PPD with SP and AM, where SP was used as an energy receptor, a multi-color fluorescence emission hydrogel was successfully constructed spanning blue, green, yellow, orange, and red, which was applied in multicolor information encryption and erasable ink.

Results and discussion

Binding modes between PPD and cucurbit[n]uril

As photoluminescent guests, PPD was synthesized and characterized by 1 H NMR, 13 C NMR spectroscopies, and high-resolution mass spectrometry (HR-MS) (Scheme S1; Figs. S1-S3). To study the CB[n]-confined photoluminescence performance, we first performed UV-vis to investigate the binding behavior of PPD with CB[n]s in aqueous solution. As the concentration of CB[7] increased, the maximum absorption wavelength of PPD was shifted from 411 nm to 407 nm (Fig. 1a). Based on the UV-vis absorption spectra, the binding constant between PPD and CB[7] was calculated as $8.04 \times 10^6 \, \mathrm{M}^{-1}$ (Fig. S6a). To further investigate the inclusion behavior, 1 H NMR titration (Fig. 1e) was performed. Due to the shielding effect of CB[7], the proton signals corresponding to the alkyl-pyridine salt moiety (labeled $\mathrm{H_a-H_g}$) exhibited an upfield shift, indicating partial encapsulation of the alkyl-pyridine



Scheme 1. Schematic illustration of the multilevel assembly mechanism of PPD, CB[7], CB[8], and SBE-βCD, as well as the photo-controlled reversible multicolor supramolecular polyrotaxane luminescent hydrogel.

J. Kong et al. Nano Today 65 (2025) 102861

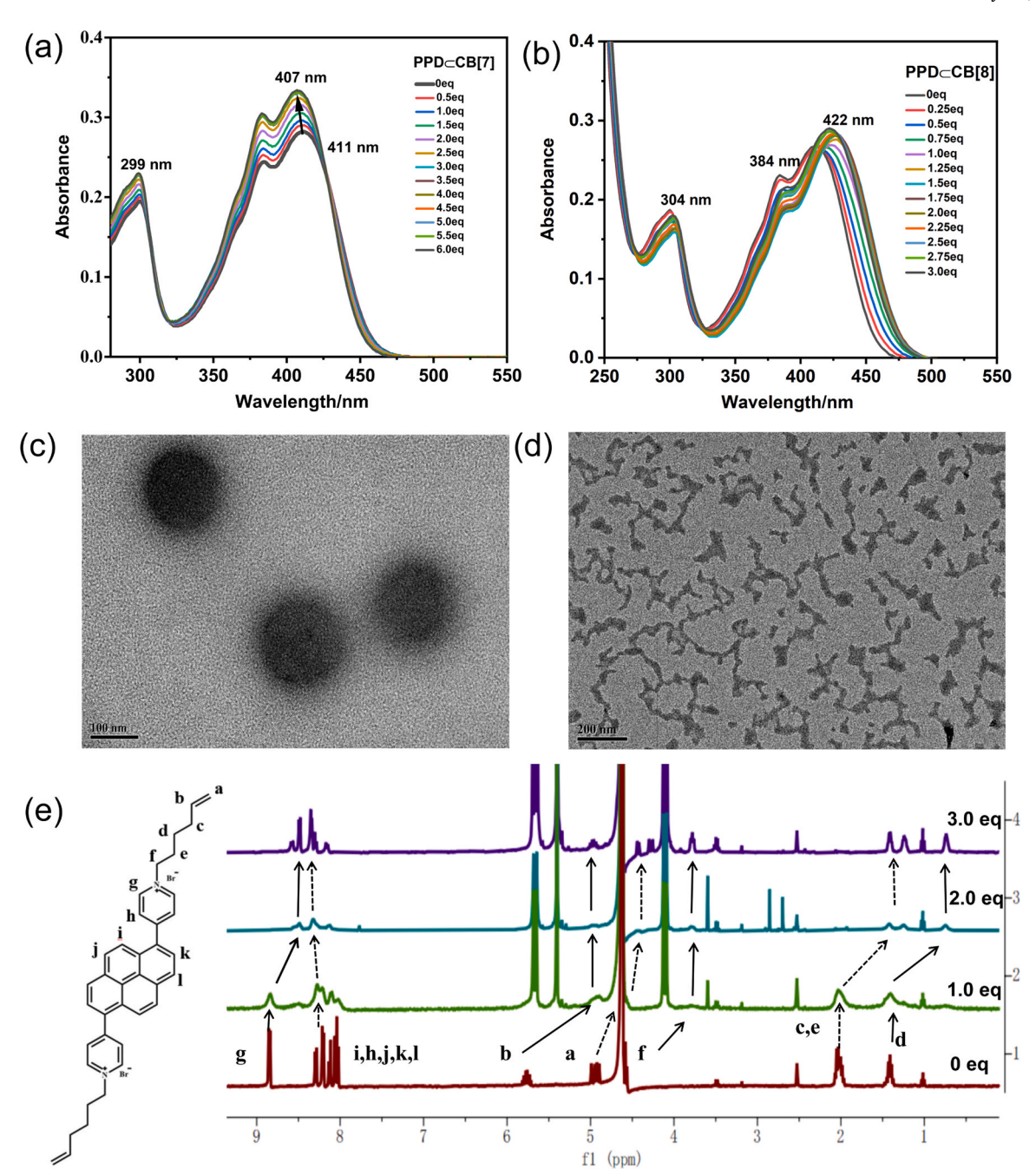


Fig. 1. UV–vis absorption spectra of PPD in aqueous solution upon the gradual addition of (a) CB[7] and (b) CB[8] at 298 K ([PPD] = 1.0×10^{-5} M). TEM image of (c) PPD \subset CB[7] and (d) PPD \subset CB[8] ([PPD] = 1.0×10^{-5} M, [CB[7]] = 2.0×10^{-5} M, [CB[8]] = 1.0×10^{-5} M). (e) 1 H NMR spectra of PPD with the addition of increasing concentrations of CB[7]. ([PPD] = 1.0×10^{-4} M, [CB[7]] = $0-3.0 \times 10^{-4}$ M, 400 MHz, D₂O, 298 K).

moiety within the CB[7] cavity. Concurrently, the H_h proton shifted downfield, demonstrating its exposure at the periphery of the CB[7] cavity. Based on the Job's plot, the stoichiometric ratio of the host-guest inclusion complex PPD:CB[7] was 1:2 (Fig. S7a). Different from CB[7], CB[8] possesses a larger cavity, which could encapsulate two positively charged PPDs. As shown by 1H NMR, upon incremental addition of CB [8] to the guest solution, the proton signals of PPD gradually broadened. When the CB[8] concentration exceeded 1 equivalent, the signals stabilized, indicating that the complexation between PPD and CB[8] reached equilibrium (Fig. S8), and the Job's plot also suggested a 1:1 stoichiometric ratio for the PPD:CB[8] complex (Fig. S7b). However, it remained unclear whether the complex adopted a simple 1:1 binding mode or the sled n:n binding mode. To confirm this, UV–vis absorption titration of PPD=CB[8] was performed. As the CB[8] concentration

increased, the absorption spectrum of PPD exhibited a red shift from 411 nm to 422 nm (Fig. 1b), consistent with J-aggregate formation upon binding to CB[8]. Based on the UV–vis absorption spectra, the binding constant between PPD and CB[8] was calculated as $1.32 \times 10^7~{\rm M}^{-1}$ (Fig. S6b). Furthermore, the assembly topological morphologies of PPDCB[7] and PPDCB[8] were characterized by transmission electron microscopy (TEM). TEM images revealed that PPD alone formed irregular nanoparticles (Fig. S9), while PPDCB[7] self-assembled into spherical nanoparticles (Fig. 1c), and PPDCB[8] was assembled into a linear structure (Fig. 1d), which was driven by the host-guest interaction between PPD and CB[n]s. The differences in topological morphologies may be attributed to the different binding mode between PPD and CB [7]/CB[8], where the sled n:n binding mode of PPDCB[8] tends to aggregate into linear polymers.

Fluorescence behavior of supramolecular cascade assembly in solution

In order to research the macrocycles confined fluorescence behavior, fluorescence titration experiments were performed, which showed that with the concentration of CB[7] increased, the fluorescence peak of PPD was blue-shifted from 526 nm to 500 nm (Fig. 2a). Under excitation with a 365 nm UV lamp, fluorescent colors ranging from green to blue can be observed in an aqueous solution. Similarly, increasing CB[8] concentration caused a red-shift of the PPD fluorescence peak from 526 nm to 534 nm (Fig. 2b), accompanied by fluorescent color changes from green to yellow. To further regulate the luminescent behavior of PPD \subset CB[n], we attempted to introduce α CD, β CD, γ CD, and SBE- β CD into the PPD \subset CB[n] assembly. Results showed that only SBE- β CD modulated the emission of PPD within the assembly (Figs. S10a, b), so that SBE- β CD was selected for secondary assembly with PPD \subset CB[n] due

to the electrostatic interactions enabled by its sulfonate groups. Upon adding SBE-βCD, the fluorescence peak of free PPD was red-shifted from 526 nm to 546 nm (Fig. S11a). For the PPDCB[7] assembly with SBE-βCD, the emission peak was red-shifted from 500 nm to 550 nm (Figs. 2c, S11b). Under 365 nm UV irradiation, the fluorescent color changed from blue to yellow in aqueous solution (Fig. 2c, inset). Similarly, the PPDCB[8] assembly with SBE-βCD exhibited a red-shift from 534 nm to 570 nm (Figs. 2d, S11c), with fluorescent colors transitioning from yellow to orange-red (Fig. 2d, inset). In addition, the quantum yield of PPDCB[7] was 74.86 %, and that of PPDCB[8] was 64.43 %, which was significantly higher than the quantum yield of PPD (54.65 %). The quantum yield of PPDCB[7]@SBE-βCD was 71.84 %. PPDCB[8]@SBE-βCD had a quantum yield of 61.93 % (Figs. S12a-e).

TEM imaging revealed that the PPDCCB[7]@SBE-βCD inclusion complex formed nanosheets with lengths of 400–800 nm (Figs. 2e,

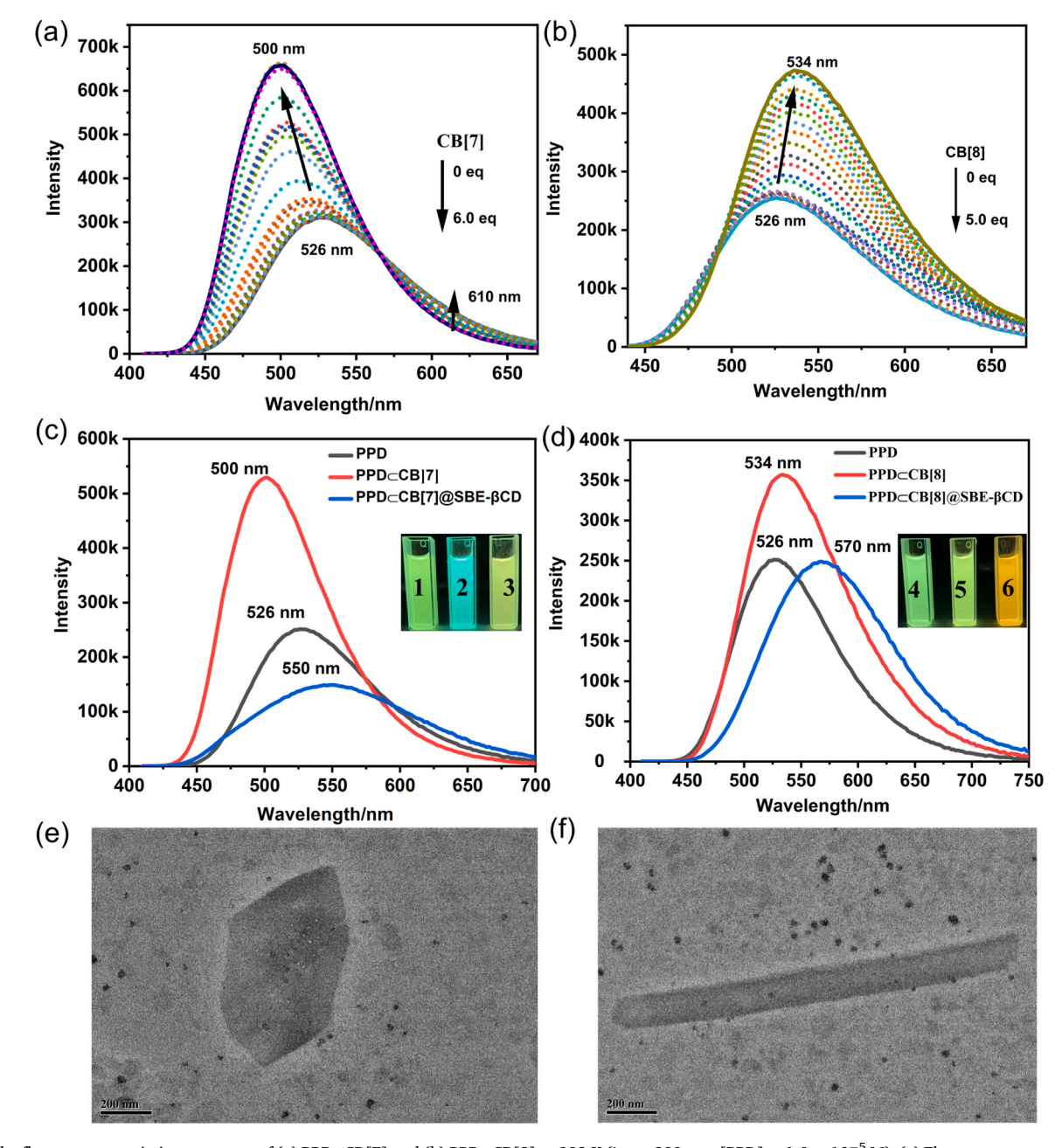


Fig. 2. The fluorescence emission spectrum of (a) PPDCCB[7] and (b) PPDCCB[8] at 298 K ($\lambda_{ex} = 390$ nm, [PPD] = 1.0×10^{-5} M). (c) Fluorescence contrast analysis of PPD, PPDCCB[7], PPDCCB[7]@SBE-βCD. Inset: Photograph from left by PPD, PPDCCB[7]@SBE-βCD upon irradiation with 365 nm UV. (d) Fluorescence contrast analysis of PPD, PPDCCB[8], PPDCCB[8]@SBE-βCD. Inset: Photograph from left by PPD, PPDCCB[8], PPDCCB[8]@SBE-βCD upon irradiation with 365 nm UV. TEM of (e) PPDCCB[7]@SBE-βCD and (f) PPDCCB[8]@SBE-βCD ([PPD] = 1.0×10^{-5} M).

J. Kong et al. Nano Today 65 (2025) 102861

\$13a), while the PPD⊂CB[8]@SBE-βCD inclusion complex selfassembled into nanorods measuring 500-1500 nm (Figs. 2 f, S13b). The topological transformation was driven by electrostatic interactions between negatively charged SBE-βCD and PDD⊂CB[n] complexes, resulting in a more compact structure. The assembly processes of SBEβCD with PPD and PPDCCB[n] were investigated by monitoring transmittance at 550 nm. In the absence of SBE-βCD, the transmittance of PPD showed no significant concentration dependence (Figs. S14a, S15a). However, with SBE-βCD, transmittance decreased sharply and stabilized at concentrations above 35 μM (Figs. S14b, S15b). This contrast indicated SBE-βCD promoted stable co-assembly through electrostatic interactions, significantly lowering the critical aggregation concentration (CAC) to 35 µM. The optimal molar ratio of PPD@SBE- βCD was determined as 1:0.64 at 50 μM PPD, where transmittance reached a minimum of 94 % (Figs. S14c, S15c). For PPD⊂CB[7]@SBEβCD, the minimum transmittance occurred at a 1:0.36 molar ratio, with no further change upon additional SBE- β CD (Figs. S14d, S15d). Similarly, PPD \subset CB[8]@SBE- β CD showed minimal transmittance at a 1:0.64 ratio (Figs. S16a, **b**).

To achieve fluorescence resonance energy transfer (FRET), we introduced SP as the energy receptor. SP was synthesized and characterized by ¹H NMR, ¹³C NMR (Scheme S2; Figs. S4-S5). First, the spectral overlap of the SP moiety was evaluated through UV–vis spectroscopy (Fig. S17a). The results demonstrated that significant spectral overlap emerged after the SP unit underwent isomerization to its merocyanine (MC) form, indicating that the MC isomer served as an ideal energy acceptor. Next, we studied the photo-controlled energy transfer between the PPDCB[7]@SBE-βCD and SP under varied UV irradiation durations. Upon 365 nm UV irradiation, the absorption peak at 500 nm progressively diminished while a new peak at 632 nm intensified. Concurrently, the solution color transitioned from yellow to red (Fig. S17b, inset). Subsequently, the irradiation of the 530 nm lamp

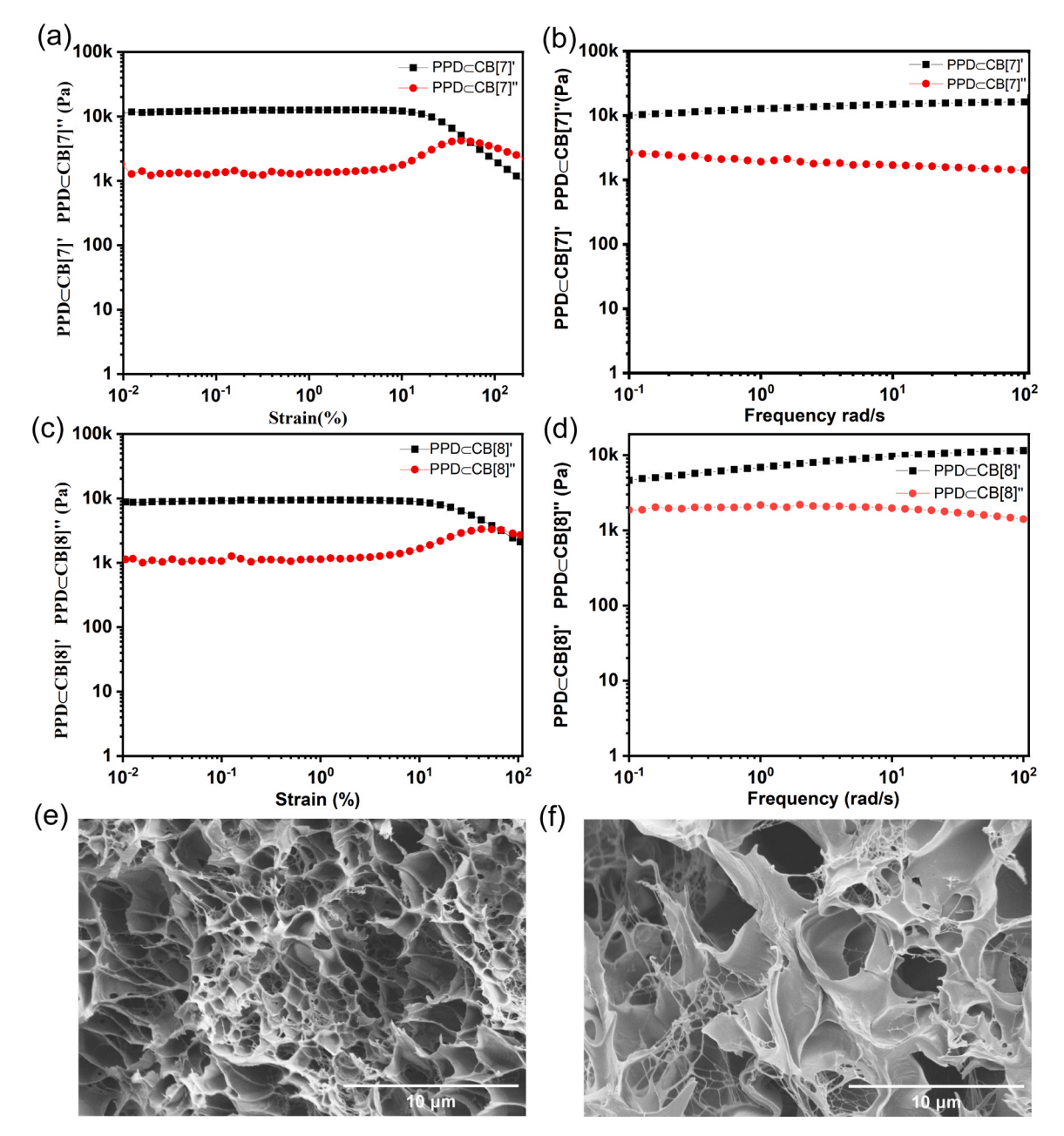


Fig. 3. (a) Strain sweep tests of PPD \subset CB[7] gel ($\gamma = 0.01-100$ %, $\omega = 6.28$ rad/s). (b) Frequency sweep tests of PPD \subset CB[7] at $\omega = 0.01-100$ rad/s and $\gamma = 1$ %. (c) Strain sweep tests of PPD \subset CB[8] gel ($\gamma = 0.01-100$ %, $\omega = 6.28$ rad/s). (d) Frequency sweep tests of PPD \subset CB[8] at $\omega = 0.01-100$ rad/s and $\gamma = 1$ %. (e) SEM image of PPD \subset CB[7] gel. (f) SEM image of PPD \subset CB[8] gel. ([PPD] = 1.0×10^{-5} M, [CB[7]] = 2.0×10^{-5} M, [CB[8]] = 1.0×10^{-5} M).

caused the 500 nm peak to recover and the 632 nm peak to attenuate, with the solution reverting to yellow color (Fig. S17c, inset). The PPDCCB[8]@SBE-βCD complex with SP exhibited analogous photoresponsive energy transfer behavior (Fig. S17d, inset).

Solid hydrogel behavior of polyrotaxane

To research the supramolecular solid hydrogel behavior, we constructed the supramolecular hydrogels through in situ copolymerization of PPD/CB[n]/AM in water. The synthetic route of the supramolecular hydrogels was described (Schemes S3-S5). The mechanical properties of supramolecular hydrogels were studied by rheological tests. When frequency(ω) = 6.28 rad/s was fixed in the rheological experiments, the no gel-to-sol state transition was observed in a wide strain region (γ <10 %, Figs. 3a, c, S18a). Moreover, according to frequency sweep test results at a fixed strain (γ) of 1 %, both PPD gel, PPD \subset CB[7] gel, and PPD \subset CB[8] gel showed higher storage modulus(PPD'/PPD \subset CB[7]'/PPD \subset CB[8]') than loss modulus (PPD''/PPD \subset CB[7]''/PPD \subset CB[8]''), implying that the gel-phase materials were stable enough and the gel structure could not be destroyed at the tested frequency range of ω = 0.01–100 rad/s (Figs. 3b, d, S18b), and the crosslink densities of PPD /PPD \subset CB[7]

/PPD \subset CB[8] were caculated as 7.31, 5.51, and 3.31 mol/m³, respectively [51]. Additionally, scanning electron microscopy (SEM) images of the freeze-dried supramolecular gels revealed a highly porous structure. The pore size of the PPD \subset CB[7] gel was approximately 2–3 μ m, larger than that of pristine PPD gel (1–2 μ m), with the PPD \subset CB[8] gel exhibiting a further enlarged pore size of 3–4 μ m. (Figs. 3e, f, S19). Notably, the prepared PPD /PPD \subset CB[7] /PPD \subset CB[8] hydrogels all demonstrated favorable stability, exhibiting no significant changes in their photoluminescence (PL) spectrum after 24 h of ambient storage. (Fig. S20).

Photo-controlled reversible luminescent behavior of supramolecular hydrogel

Building upon these intriguing experimental observations, SP was introduced as the energy acceptor to fabricate photo-controlled supramolecular rotaxanes through in situ copolymerization with PPDCB[7], AM, and methyl acrylate. The synthetic route of the supramolecular hydrogels was described. We systematically investigated the photoregulated FRET behavior between the PPDCB[7] supramolecular hydrogel and SP under alternating UV light irradiation. Upon 365 nm UV irradiation, the absorption peak at 500 nm progressively diminished,

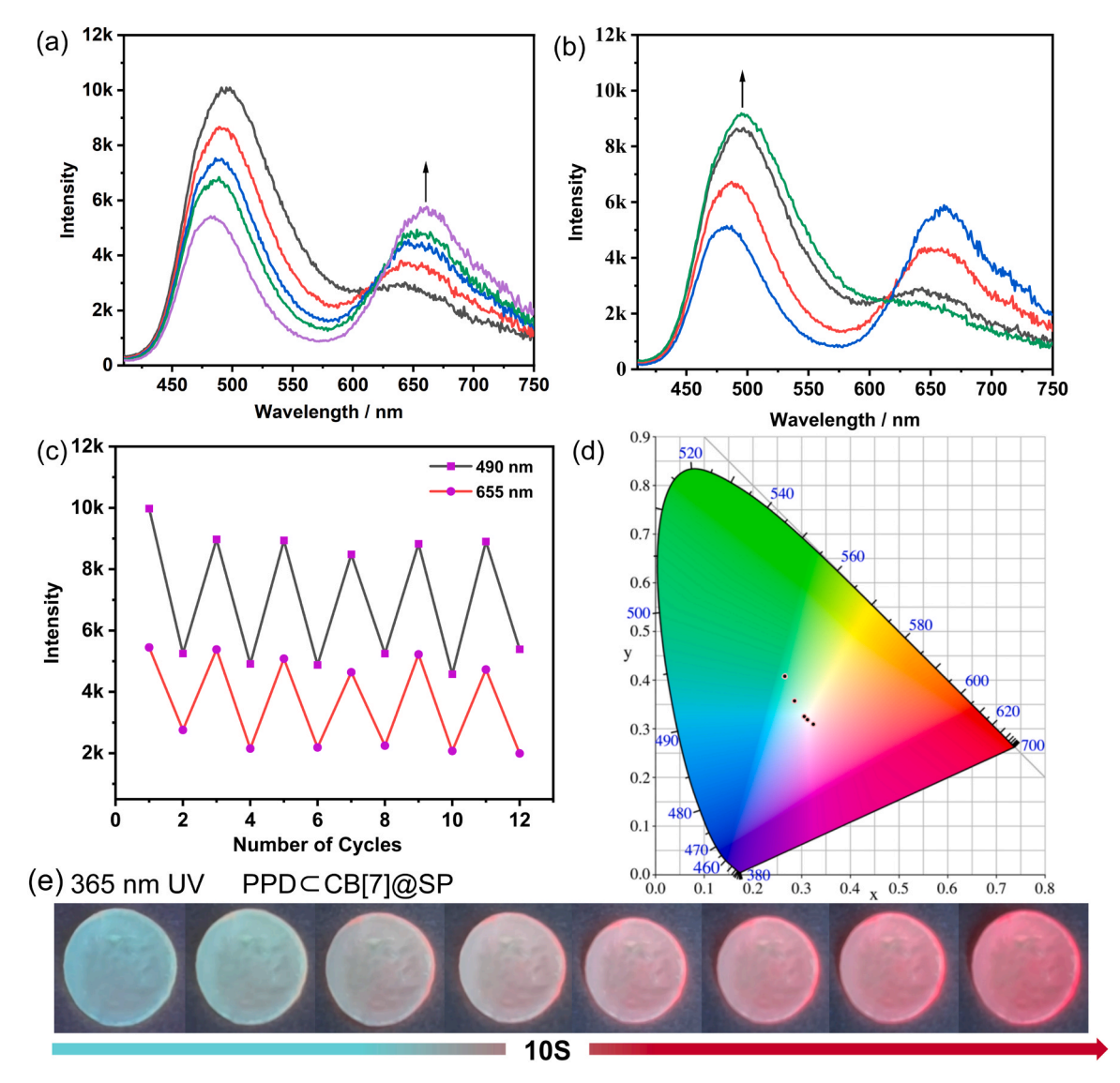


Fig. 4. (a) Fluorescence spectra of PPD \subset CB[7]@SP gel under 365 nm UV light ($\lambda_{ex} = 390$ nm). (b) Fluorescence spectra of PPD \subset CB[7]@SP gel under 530 nm light. (c) Emission intensity changes at 490 nm and 655 nm. (d) 1931 CIE chromaticity diagram of PPD \subset CB[7]@SP gel upon alternating 365 nm UV lamp. (e) Under the irradiation of a 365 nm UV lamp, the color of the PPD \subset CB[7]@SP gel changes.

accompanied by the emergence of a new absorption band at 655 nm (Fig. 4a). Subsequent exposure to 530 nm visible light, the 500 nm peak intensity was restored, and the 655 nm signal was attenuated (Fig. 4b), and the fluorescence emission changes can be cycled more than five times without obvious fatigue under alternating 365 nm and 530 nm light irradiation (Fig. 4c). The direction of fluorescence the color change was confirmed in the CIE in the 1931 chromaticity chart, from (0.264, (0.407) to (0.311, 0.319) irradiation (Fig. 4d), in which the color of the fluorescence changed from blue to yellow to red under 365 nm irradiation can also be observed through naked-eye and portable cameras (Fig. 4e). This dynamic optical modulation enabled the successful development of reversibly multicolor luminescent hydrogels, achieving programmable and precise fluorescence switching between blue and red emission. SEM analysis further confirmed that with the incorporation of SP as an energy acceptor, the hydrogel maintained a dense and uniform porous structure. This confined environment resulted in a slower ringopening/closing reaction rate of SP compared to in solution, laying the foundation for subsequent information anti-counterfeiting applications. Moreover, during the reversible ring-opening/closure isomerization of SP, the internal structural changes of the hydrogel were negligible (Fig. S21).

Information encryption and erasable ink of supramolecular Hydrogels

Although the PPD, PPDCB[n], and PPDCB[n]@SBE-βCD solutions exhibited similar pale-yellow coloration, their photoluminescent behaviors differed significantly, enabling their application in information storage. By utilizing diverse assembly modes, the 520NK patterns were indistinguishable under daylight but became discernible under 365 nm

irradiation (Fig. 5a). For cryptographic encryption, PPDCCB[7]@SP hydrogel encoded critical information, while non-critical regions were replaced with PPDCB[7] hydrogel. Under 365 nm illumination, encrypted information emerged as red fluorescence, which gradually reverted to its original state upon 530 nm irradiation. After being exposed to a 365 nm irradiation, the encrypted information 302 was displayed (Fig. 5b). Unlike unidirectional anti-counterfeiting systems, the bidirectionally reversible multicolor rotaxane system demonstrated the potential for dynamic information storage and encryption. Fluorescent patterns with encoded messages can be fabricated through information-loading and decryption processes. Besides, when a custommade photomask was applied to the rotaxane system, a cartoon image was obtained after 40 s of 365 nm irradiation. Regions exposed to visible light emitted red fluorescence, while masked areas showed blue fluorescence. Subsequent irradiation with 530 nm light can erase the image, achieving information deletion. Notably, the reversibility of the multicolor rotaxane architecture allowed cyclic information erasure and rewriting, facilitating the sequential generation of target patterns (Fig. 5c). Moreover, it can be used for fabricating time multicolor gel changes with time, and the cartoon-shaped hydrogel kept changing from blue to yellow, orange, and then to red under 365 nm UV irradiation (Fig. 5d).

Conclusion

From the above research, we can summarize that macrocycles CB[n]s can not only regulate supramolecular topological morphology but also efficiently enhance fluorescence behavior. Through the supramolecular cascade assembly of PPD, CB[n], and SBE- β CD, we successfully

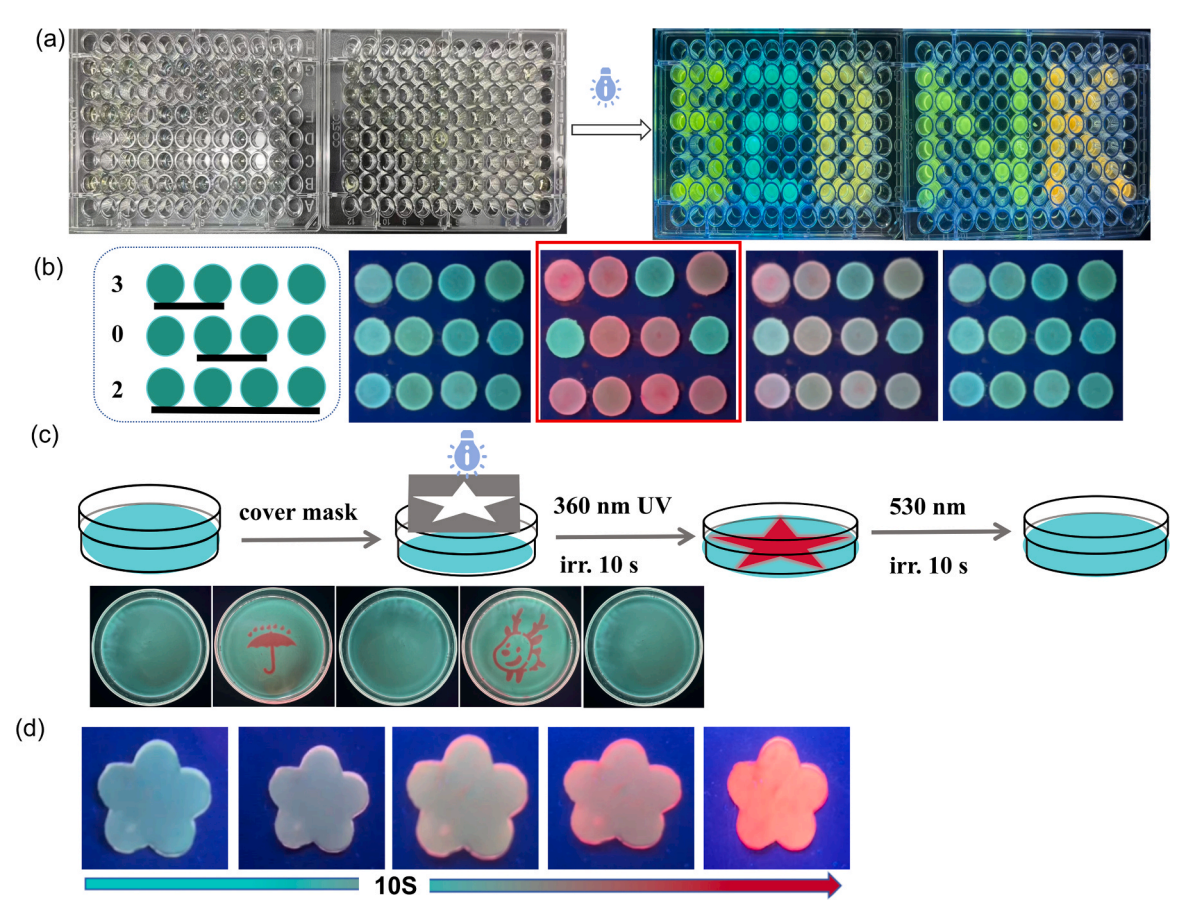


Fig. 5. (a) Information storage of PPD, PPD⊂CB[7], PPD⊂CB[7]@SBE-βCD, PPD⊂CB[8], PPD⊂CB[8]@SBE-βCD, under daylight and 365 nm UV irradiation. (b) '302' via Morse code under light irradiation. (c) Schematic diagram and under UV lamp of the construction of writable and self-erasing PPD⊂CB[7]@SP supramolecular hydrogel. (d) Under the irradiation of 365 nm UV, the color of the PPD⊂CB[7]@SP supramolecular hydrogel changes.

J. Kong et al. Nano Today 65 (2025) 102861

constructed reversibly multicolor fluorescent supramolecular rotaxane and polyrotaxane systems. The host-guest interactions with CB[n] enabled programmable polychromatic fluorescence emission. The primary assembly PPDCB[7] exhibited enhanced blue fluorescence at 500 nm. Subsequent electrostatic assembly with SBE-βCD resulted in fluorescence quenching and red-shift to 550 nm for the PPDCCB[7] @SBE-βCD complex, accompanied by the formation of nanosheets. Similarly, the PPDCCB[8] assembly displayed intensified vellow fluorescence at 534 nm, which further red-shifted to 570 nm upon hierarchical SBE-βCD integration, yielding rod-like nanostructures. Remarkably, the introduction of SP into the PPDCB[n] through in situ copolymerization with AM and methyl acrylate activated RET, generated near-infrared fluorescence at 655 nm. This strategy achieved a color-tunable supramolecular rotaxane system with reversible blue-tored fluorescence switching. The resultant system demonstrated promising applications in dynamic information storage through optically regulated fluorescence coding. With in-depth research, supramolecular hydrogels are anticipated to enable multi-stimuli-responsive encryption platforms by integrating optical properties manipulation with shapemorphing and self-healing capabilities.

Experimental section

Materials: All reagents and solvents were available from commercial sources and used directly without any purification.

Transmission Electron Microscopy (TEM): A 10 μ L sample solution (PPD = 1×10^{-5} M, CB[7] = 2×10^{-5} M, CB[8] = 1×10^{-5} M, SBE- β CD = 1×10^{-5} M) was carefully drop-cast into a pristine copper grid. After air-drying under ambient conditions, Photographs were then taken using TEM.

Scanning electron microscope (SEM): Prepare solution (PPD = 1×10^{-5} M, CB[7] = 2×10^{-5} M, CB[8] = 1×10^{-5} M), lyophilized, Photographs were then taken using TEM.

Synthesis of compounds PPD \subset CB[7]@SP hydrogel: In 3 mL of water PPD (1 \times 10⁻⁵ M) and CB[7] (2 \times 10⁻⁵ M) were assembled, followed by the addition of Tween 80 aqueous solution (1 mL). SP (1 \times 10⁻³ M) was dissolved in methyl acrylate (30 μ L) and then added to the solution, followed by vortexing for 10 min to form a homogeneous emulsion. AM (500 mg) was added to the emulsion, and the mixture was vortexed for an additional 10 min. Ammonium persulfate (5 mg) was added as a thermal initiator, and the system was placed in an 80 °C oven for 1 h to prepare PPD \subset CB[7]@SP hydrogel.

CRediT authorship contribution statement

Chen Zhang: Software. Chu-Han Liu: Software. Yu Liu: Supervision, Funding acquisition. Jing Kong: Writing – original draft, Investigation, Data curation. Shuang-Qi Song: Software, Methodology, Data curation. Man Huo: Formal analysis.

Declaration of Competing Interest

The authors declare that they have no known competing financial interests or personal relationships that could have appeared to influence the work reported in this paper.

Acknowledgments

The authors thank the National Natural Science Foundation of China (NNSFC, Grant Nos. 22131008), and China Fundamental Research Funds for the Central Universities for financial support.

Author Agreement Statement

We the undersigned declare that this manuscript is original, has not been published before and is not currently being considered for publication elsewhere.

We confirm that the manuscript has been read and approved by all named authors and that there are no other persons who satisfied the criteria for authorship but are not listed. We further confirm that the order of authors listed in the manuscript has been approved by all of us.

We understand that the Corresponding Author is the sole contact for the Editorial process. He/she is responsible for communicating with the other authors about progress, submissions of revisions and final approval of proofs

Appendix A. Supporting information

Supplementary data associated with this article can be found in the online version at doi:10.1016/j.nantod.2025.102861.

Data availability

Data will be made available on request.

References

- [1] A. Jozeliu naitė, T. Javorskis, V. Vaitkevičius, V. Klimavičius, E. Orentas, J. Am. Chem. Soc. 144 (2022) 8231–8241.
- [2] Y.-Q. Li, X. Zhang, J.-Y. Zheng, Y. Zhou, W.-Q. Huang, Y.-P. Song, H. Wang, X.-Y. Song, J.-H. Luo, S.-G. Zhao, Angew. Chem. Int. Ed. 62 (2023) e202304498.
- [3] A.-L. Huang, H.-S. Yang, S.-M. Huang, G.-S. Chen, G.-F. Ouyang, Matter 6 (2023) 2635–2646.
- [4] T. Meng, P. Zhang, H.-M. Zhong, H.-D. Zhu, H. Zhang, D.-Y. Xu, Y. Zhao, Nano Lett. 24 (2024) 14095–14101.
- [5] S.-Q. Song, H.-Z. Zhang, Y. Liu, Acc. Mater. Res. 5 (2024) 1109-1120.
- [6] H.-T. Zhu, L.-Y. Chen, B. Sun, M.-B. Wang, H. Li, J.F. Stoddart, F.-H. Huang, Nat. Rev. Chem. 7 (2023) 768–782.
- [7] M.-M. Yan, S. Wu, Y.-H. Wang, M.-H. Liang, M.-B. Wang, W.-T. Hu, G.-C. Yu, Z.-W. Mao, F.-H. Huang, J. Zhou, Adv. Mater. 36 (2024) 2304249.
- [8] D.-F. Li, F.-F. Lu, J. Wang, W.-D. Hu, X.-M. Cao, X. Ma, H. Tian, J. Am. Chem. Soc. 140 (2018) 1916–1923.
- [9] C.B. Kc, F. D'Souza, Coord. Chem. Rev. 322 (2016) 104-141.
- [10] S.M. Jansze, K. Severin, Acc. Chem. Res. 51 (2018) 2139–2147.
- [11] L. Liang, W. Zhao, X.-J. Yang, B. Wu, Acc. Chem. Res. 55 (2022) 3218-3229.
- [12] M. Chafiq, A. Chaouiki, J. Ryu, Y.G. Ko, Nano Today 56 (2024) 102227.
- [13] M.-J. Jiang, X.-Y. Wang, Y.-H. Zhang, J. Wang, J. Kang, B.-L. Wang, A. Dong, Y. Liu, Nano Today 61 (2025) 102614.
- [14] X. Zhao, X.-L. Zhou, Q.-W. Cheng, Y. Liu, Nano Today 60 (2025) 102561.
- [15] Q. Wang, H.-R. Xu, Z. Qi, J. Mei, H. Tian, D.-H. Qu, Angew. Chem. Int. Ed. 63 (2024) e202407385.
- [16] B.-Y. Lin, Q. Wang, Z. Qi, H.-R. Xu, D.-H. Qu, Sci. China Chem. 66 (2023) 1111–1119.
- [17] Q. Wang, Z. Qi, Q.-M. Wang, M. Chen, B.-Y. Lin, D.-H. Qu, Adv. Funct. Mater. 32 (2022) 2208865.
- [18] W.-C. Geng, Z.-J. Ye, Z. Zheng, J. Gao, J.-J. Li, M.R. Shah, L.-H. Xiao, D.-S. Guo, Angew. Chem. Int. Ed. 60 (2021) 19614–19619.
- [19] J. Yu, J. Niu, J.-L. Yue, L.-H. Wang, Y. Liu, ACS Nano 17 (2023) 19349–19358.
- [20] X.-J. Yan, F.-H. Ma, Q.-X. Chen, X.-B. Gou, X.-H. Li, L.-W. Zhang, H. Gao, Chem. Eng. J. 450 (2022) 137605.
- [21] J.-Q. Li, Y. Zhang, S.-E. Liu, J. Niu, R. Zhang, Y. Chen, Y. Liu, Chin. Chem. Lett. 35 (2024) 109645.
- [22] J.-J. Han, H.-D. Li, J.-Y. Yoon, Nano Today 43 (2022) 101392.
- [23] X.-Y. Dai, M. Huo, Y. Liu, Nat. Rev. Chem. 7 (2023) 854-874.
- [24] X.-Y. Dai, Y.-Y. Hu, Y.-H. Sun, M. Huo, X.-Y. Dong, Y. Liu, Adv. Sci. 9 (2022) 2200524.
- [25] Y. Xia, S.-Y. Chen, X.-L. Ni, ACS Appl. Mater. Interfaces 10 (2018) 13048–13052.
- [26] Q.-L. Zhou, H.-S. Wang, L. Liu, B. Dong, L.-H. Sun, X.-D. Niu, Nano Today 62 (2025) 102733.
- [27] W. Zhang, Y. Luo, C. Liu, M.-X. Yang, J.-X. Gou, Y. Huang, X.-L. Ni, Z. Tao, X. Xiao, ACS Appl. Mater. Interfaces 14 (2022) 51429–51437.
- [28] O.-C. Lu, N.-N. Li, X.-M. Zhang, Chem. Eng. J. 436 (2022) 132889.
- [29] Y.-Q. Wang, A.M. Bimmermann, M. Neufurth, P. Besenius, Adv. Mater. 36 (2024) 2313270.
- [30] Y.-H. Sun, L.-N. Jiang, Y. Chen, Y. Liu, Chin. Chem. Lett. 35 (2024) 108644.
 [31] Z.-Y. Wang, S.-J. Jia, H.-L. Xu, B.-T. Lu, W.-D. Wu, Y.-X. Ai, Y.-J. Liu, R.-F. Liu, Y.-
- [31] Z.-Y. Wang, S.-J. Jia, H.-L. Xu, B.-T. Lu, W.-D. Wu, Y.-X. Ai, Y.-J. Liu, R.-F. Liu, Y.-L. Cao, S.-X. Cheng, C.-P. Hu, Z.-M. Yang, L. Zhu, D.-J. Hao, Nano Today 51 (2023) 101894.
- [32] M. Colaço, J. Ewert, J.-S. von Glasenapp, U. Pischel, R. Herges, N. Basílio, J. Am. Chem. Soc. 147 (2025) 734–745.
- [33] L.-R. Yang, Y.-X. Li, H.-F. Zhang, C.-M. Tian, Q.-H. Cao, Y.-M. Xiao, L.-B. Yuan, G.-X. Liu, Chin. Chem. Lett. 34 (2023) 108108.
- [34] W. Lee, D. Kim, S. Lee, J. Park, S. Oh, G. Kim, J. Lim, J. Kim, Nano Today 23 (2018) 97–123.
- [35] H.-L. Chen, W.-N. Zhang, S.-Z. Ren, X.-A. Zhao, Y. Jiao, Y. Wang, J.F. Stoddart, X.-F. Guo, Adv. Mater. 34 (2022) 2101487.

- [36] Z.-A. Bai, H.-T. Zhang, R. Xue, X.-L. Lu, X.-Y. Li, W. MacSwain, W. Zheng, J.-Q. Xu, Y. Yu, Y.-L. Bai, Aggregate 5 (2024) e583.
- [37] M.-R. Zhang, Y.-J. Cheng, T. Zhang, B.-C. Liang, X.-H. Wei, P. Wang, D.-Y. Xia, X.-Z. Yan, Aggregate 5 (2024) e608.
- [38] M.-Z. Chen, H. Hu, X. Cheng, Y. Wu, Z.-M. Ma, R.P. Sijbesma, Z.-Y. Ma, Adv. Opt. Mater. 12 (2024) 2400733.
- [39] X.K. Ma, W. Zhang, Z.X. Liu, H.Y. Zhang, B. Zhang, Y. Liu, Adv. Mater. 33 (2021) 2007476.
- [40] X.-L. Zhou, X. Bai, X.-J. Zhang, J. Wu, Y. Liu, Adv. Opt. Mater. 12 (2024) 2301550.
- [41] Y.-T. Kang, X.-Y. Tang, H.-D. Yu, Z.-G. Cai, Z.-H. Huang, D. Wang, J.-F. Xu, X. Zhang, Chem. Sci. 8 (2017) 8357–8361.
- [42] X.-Y. Tang, Z.-H. Huang, H. Chen, Y.-T. Kang, J.-F. Xu, X. Zhang, Angew. Chem. Int. Ed. 57 (2018) 8545–8549.

- [43] X.-L. Ni, S.-Y. Chen, Y.-P. Yang, Z. Tao, J. Am. Chem. Soc. 138 (2016) 6177–6183.
- [44] M.-D. Tian, Z. Wang, X. Yuan, H. Zhang, Z.-X. Liu, Y. Liu, Adv. Funct. Mater. 33 (2023) 2300779.
- [45] M. Huo, X.-Y. Dai, Y. Liu, Adv. Sci. 9 (2022) 2201523.
- [46] Z.-X. Liu, H.-Q. Chen, M.-D. Tian, X.-Y. Sun, Y.-X. Li, J. Wu, R.-T. Wang, B. Li, C.-J. Li, Y. Liu, Aggregate 5 (2024) e627.
- [47] S.-Q. Song, H.-Z. Zhang, Y. Liu, Acc. Mater. Res. 5 (2024) 1109–1120.
- [48] X.-L. Yu, A.A. Ryadun, D.I. Pavlov, T.Y. Guselnikova, A.S. Potapov, V.P. Fedin, Adv. Mater. 36 (2024) 2311939.
- [49] M.-Q. Du, C. Li, Adv. Mater. 36 (2024) 2408484.
- [50] R. Zhang, Y. Chen, Z.-Y. Yu, Y. Liu, Chin. Chem. Lett. (2025) 111147.
- [51] S. Piskounova, R. Rojas, K. Bergman, J. Hilborn, Macromol. Mater. Eng. 296 (2011) 944–951.